[Frontiers in Bioscience 9, 505-512, January 1, 2004]

TIME PROFILE OF CEREBRAL [18F]6-FLUORO-L-DOPA METABOLITES IN NONHUMAN PRIMATE: IMPLICATIONS FOR THE KINETICS OF THERAPEUTIC L-DOPA

Christopher J. Endres [1], Onofre T. DeJesus [1], Hideo Uno [3], Doris J. Doudet [4], R. Jerome Nickles [1,2], and James E. Holden [1,2]

Departments of [1] Medical Physics, [2] Radiology, University of Wisconsin Medical School and the [3] Wisconsin Regional Primate Research Center, Madison, WI 53706, [4]Department of Medicine, Division of Neurology, University of British Columbia, Vancouver, BC, Canada

TABLE OF CONTENTS

1. ABSTRACT

At least two rates of dopamine turnover have been demonstrated *in vivo*, including a slow turnover rate that is associated with synaptic vesicles, and a faster rate that leads to rapid production of dopamine metabolites. Similarly, [^{18}F]6-fluorodopamine (FDA), the decarboxylation product of the PET tracer [^{18}F]6-fluoro-L-DOPA (FDOPA), may have multiple turnover rates which could substantially affect the interpretation of FDOPA uptake. To better characterize FDA turnover *in vivo*, we measured the formation of FDOPA metabolites in primate brain following bolus FDOPA injection with carbidopa pretreatment. FDOPA was allowed to circulate for either 30 minutes or 90 minutes, prior to removal of brain samples. The primary metabolites in striatum were [^{18}F]6-fluoro-3-methyl-L-DOPA (3-OMFD), FDA, [^{18}F]6-fluoro- L-3,4-dihydroxyphenylacetic acid (FDOPAC), and [^{18}F]6-fluorohomovanillic acid (FHVA). The percentages of total radioactivity in striatum at 30 minutes and 90 minutes were: FDOPA(5%, 2%), FDA (39%, 23%), FDOPAC (12%, 3%), FHVA (14%, 34%), and 3-OMFD (29%, 39%). In cortex and cerebellum most of the activity (73%, 80%) was 3-OMFD. These data were compared against the metabolite profiles predicted by two compartmental models of FDOPA metabolism. A model that assumes only a single slow rate of FDA turnover predicted much lower concentrations of FDA metabolites (FDOPAC, FHVA) in striatum than were found in the brain assay, while a model that includes both slow and fast FDA turnover was in much better agreement. These findings extend and confirm previous observations of FDOPA metabolites. The implications for the interpretation of FDOPA PET, particularly in terms of the availability of dopamine synthesized from therapeutic L-DOPA, are discussed.

2. INTRODUCTION

The kinetics of cerebral [^{18}F]6-fluoro-L-DOPA (FDOPA) measured *in vivo* by PET feature the nearly irreversible accumulation of radioactivity in dopaminergic neurons. This accumulation follows decarboxylation of FDOPA by aromatic amino acid decarboxylase (AAAD), (Figure 1) and thus quantitative measurements of the FDOPA accumulation rate are usually interpreted as reflecting AAAD activity (1-5). The decarboxylation product of FDOPA is [^{18}F]6-fluorodopamine (FDA), which behaves *in vivo* very similarly to dopamine. For example, FDA is metabolized via monoamine oxidase (MAO) to yield [^{18}F]6-fluoro-L-3,4-dihydroxyphenylacetic acid (FDOPAC), and subsequently by catechol O-methyl transferase (COMT) to yield [^{18}F]6-fluorohomovanillic acid (FHVA). These [^{18}F]-labeled compounds are analogs of corresponding metabolites in the dopamine pathway, and their presence has been confirmed in the striata of rats (6,7) and monkeys (8-10). The COMT product of FDA, [^{18}F]6-fluoro-3-methoxy-tyramine (6F-3MT), has been detected in rat brain (6). Another important similarity to dopamine is that FDA is evidently stored in synaptic vesicles (11-14). Given the complexity of FDOPA metabolism and turnover,

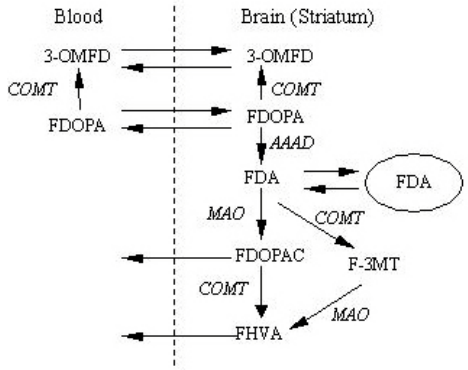

Figure 1. The metabolic fate of FDOPA. The vertical dashed line signifies the blood-brain barrier. Anatomical subcompartments in the brain are ignored with the exception of the FDA protected from metabolism by storage in vesicles, signified by the surrounding ellipse. Enzyme catalyzed reactions are labeled with the associated enzyme name in italics. The full names of all compounds and enzymes are provided in the text. All processes described in the introductory paragraphs are shown, with the addition of the COMT–catalyzed metabolism of FDOPA to 3-O-methyl-fluorodopa (3OMFD) in both periphery and brain.

there is concern that interpreting the kinetics of FDOPA solely in terms of decarboxylation and storage may be inadequate. Striatal kinetics measured with PET indeed show that the radioactivity enters a slow turnover pool, which would be consistent with the storage of FDA in synaptic vesicles. However, based on the *in vivo* behavior of dopamine, FDA may be expected to have both slow and rapid turnover components (15). For example, rapid dopamine turnover has been demonstrated in rat studies showing that a substantial amount of DOPAC is derived from newly synthesized dopamine (16,17). DOPAC is not formed in synaptic vesicles (18), and is rapidly cleared from the brain (19,20). Furthermore, the turnover of FDA in rat brain is even more rapid than the turnover of dopamine (21,22). Compartmental modeling of rat biochemical data also supports the existence of rapid FDA turnover, in addition to the slow turnover associated with vesicles (14).

To better understand the dynamics of FDOPA trapping and the *in vivo* turnover of FDA, we assayed for radioactive metabolites in the brains of four stumptail monkeys (*Macaca Arctoides*) following bolus injection of FDOPA with carbidopa pretreatment. The metabolite profile was characterized for FDOPA circulation times of 30 minutes (n=2) and 90 minutes (n=2), which provided data at both early and late time points with respect to the typical duration of a PET scan. The chosen times also complement an earlier study in which the FDOPA metabolite profile was determined in *Macaca Nemestrina* monkeys at 60 minutes post-injection (10). These data serve as a basis for examining compartmental models of FDOPA metabolism. This study will help to better characterize FDA turnover *in vivo*, which can improve the physiological interpretation of FDOPA uptake.

3. MATERIALS AND METHODS

3.1. Animal subjects

Four *Macaca Arctoides* Monkeys (Table 1) were sedated with 10mg/kg ketamine and then anesthetized by 2.5-3.0% isoflurane and 1.6-2.0 l/min O_2 during the uptake period. Carbidopa (2 mg/kg) was administered less than one hour before FDOPA (2-5 mCi) injection. Following bolus administration, FDOPA was allowed to circulate for 30 min (n=2) or 90 min (n=2), at which times the monkeys were sacrificed under deep barbiturate anesthesia by occlusion of the ascending aorta. Brains were dissected in about 15 minutes and the tissue samples were excised and kept cool on dry ice. The brain tissues sampled were caudate, putamen, occipital cortex, frontal cortex, and cerebellum. Blood was also assayed for metabolites in all but one of the monkeys. A small portion of each tissue (1-6 gm) was placed in a pre-weighed test tube in order to measure the absolute radioactivity concentration. The remainder of the sample was homogenized in a cold solution (1-3 mL) containing 7% perchloric acid, 1 μM sodium EDTA, and 1 mg/mL sodium bisulfite. The homogenate from each tissue was poured in 1-1.5 mL aliquots into vials containing 50 μL 4M PCA and 50 μL 7.5% EDTA. The vials were then centrifuged and the supernatant was used for HPLC analysis. Injectable carbidopa was a generous gift from Merck.

3.2. Tracer Preparation

To prepare [^{18}F]FDOPA, [^{18}F]F_2 is bubbled into a solution of a mercurated protected L-DOPA derivative (BOZ Chemicals and Engineering, Montreal, Quebec, Canada) using the method of Adam and Jivan (23). [^{18}F]FDOPA was purified using a semi-preparative HPLC (Alltech C18 column, 10microns, 250x10mm). The mobile phase consisted of 0.02M NaOAc, pH 3.5, and was made up with sufficient NaCl to be isotonic. The HPLC fraction containing the product was sterilized by filtration through a 0.22μ filter prior to administration.

3.3. Tissue assay

The HPLC system consisted of a Rainin HPX solvent delivery system with the following mobile phase: 95% 0.5 M ClHOAc, 0.625 M NaOH, 0.22 M Citric Acid, 13.5 mM EDTA, 10 mM Sodium Octyl Sulfate, 17.6 μM Butylamine; 5% MeOH. A C_{18} reverse-phase column (15 cmx4.6 mm, 5 μm; Alltech) was used, with the working electrode set to an applied potential of +0.70V. Radioactivity was detected using a flow through triple coincidence detection system that binned the counts in ten-second intervals (24). Radioactive peaks were identified by comparison of the retention times to that of cold standards of FDOPA and its metabolites. The identified peaks were FDOPA, 3-OMFD, FDA, 6-[^{18}F]fluorodopamine sulfate (FDA-sulfate), FDOPAC, and FHVA. The results are expressed as peak percent of the total radioactivity in each sample, and have been decay corrected to account for the difference in elution times. The recoveries of the metabolites during the extraction procedure were not significantly different (20) and thus no corrections were made.

Table 1. Summary of monkeys used for tissue assay

Name	Sex	Age(yr)	Wt (kg)	Time(min)
M1	F	13.1	12.4	90
M2	M	10.3	13.6	30
M3	F	21.1	14.1	30
M4	F	27.8	11.5	90

Four monkeys were used for the assay of cerebral radioactive metabolites, which were measured following FDOPA circulation times of 30 minutes (n=2) and 90 minutes (n=2). The monkeys had similar weight, but a relatively wide age range. To reduce the confounding effects of age on FDOPA metabolism, the monkeys were roughly grouped as young (M1, M2) and old (M3, M4), and one monkey from each age group was studied at each circulation time.

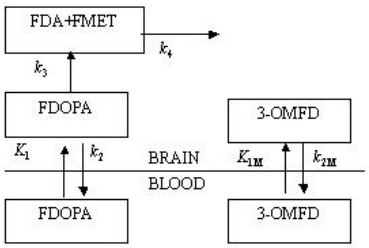

Figure 2. Basic compartmental model of FDOPA metabolism (2). FDOPA and 3-OMFD are exchanged between blood plasma and brain by the first-order processes shown. The arrow labeled k3 represents the first-order process of decarboxylation; however, free and stored FDA, and all FDA metabolites, are combined into a single well-mixed compartment capable of leaving the brain by the first order loss rate k4.

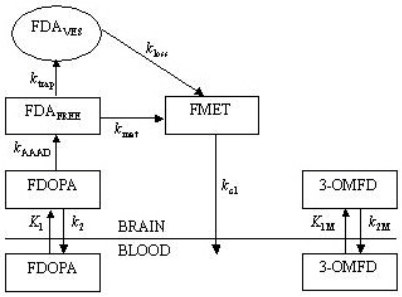

Figure 3. Expanded compartmental model of FDOPA metabolism. Separate tissue compartments are included for FDOPA, FDA that is free in tissue (FDA_{FREE}), FDA stored in synaptic vesicles (FDA_{VES}), FDA metabolites (FMET= FDOPAC+FHVA), and 3-OMFD. The designated compounds were all detected in the tissue assay. The first-order processes associated with exchange across the blood-brain barrier are identical to those in Figure 1. Decarboxylation is now denoted by k_{AAAD} . The product is divided by the competing processes of vesicular storage (k_{trap}) and rapid metabolism of free FDA (k_{met}). The remaining processes are the slow loss rate of FDA from vesicles into the metabolite compartment (k_{loss}), and the clearance of FDA metabolites from the brain (k_{CL}). The model shown with all parameters included is referred to in the text as Model II. For Model I k_{met} is set to zero.

3.4. Compartmental modeling

Compartmental models of FDOPA metabolism were examined for consistency with both FDOPA kinetics and tissue FDOPA metabolites. The purpose of this modeling effort was to determine whether the inclusion of a metabolite compartment, and provision for rapid FDA metabolism, could produce a simple model that could account simultaneously for both the tissue assay results and the kinetics of FDOPA measured by PET. We applied a model adapted from previously reported models, with a compartmental configuration arbitrarily selected as the simplest that could account for both slow and rapid FDA turnover. Representative FDOPA time-activity curves (TACs) and a metabolite corrected blood input function were drawn from the research program of Dr. Doudet at the University of British Columbia/TRIUMF PET center. A two-hour study was performed in a normal rhesus monkey that was pretreated with 5 mg/kg carbidopa. FDOPA TACs from a rhesus monkey were selected to complement the tissue assay in stumptail monkeys, because these two primate species are similar in size and weight. To ensure the selected TACs were in accord with previously reported FDOPA kinetics, TACs were first fitted to the basic FDOPA kinetic model shown in Figure 2 (2). The model parameters are the tissue exchange parameters for FDOPA (K_1, k_2), and 3-OMFD (K_{1M}, k_{2M}), the rate of uptake into the trapped compartment (k_3), and the slow loss rate (k_4). The trapping rate (k_3) is often interpreted as decarboxylase activity and is set to zero for modeling of the occipital cortex. It is assumed that the exchangeable volume of distribution (V_e) is equal for both FDOPA and 3-OMFD, thus $V_e=K_1/k_2=K_{1M}/k_{2M}$. The first fitting step was to estimate a blood-tissue time offset (Δt) by fitting the cortical TAC from 0-30 minutes. With Δt fixed, the same TAC was then fitted from 0-120 minutes in order to estimate K_1, V_e, K_1/K_{1M}, and blood volume (V_b). For modeling of the striatum, the values of V_e, K_1/K_{1M}, and Δt were held fixed to those determined in cortex, leaving 4 parameters (K_1, k_3, k_4, V_b) to be estimated.

The extended models are shown in Figure 3. For one model (Model I) FDA turnover occurs at a single slow rate that is associated with vesicles (k_{met} equal to zero), and for the other model (Model II), FDA has both slow and fast turnover. These models were adapted from previously reported FDOPA kinetic models (21); they include separate compartments for FDOPA, FDA that is freely diffusible (FDA_{FREE}), FDA that is stored in vesicles (FDA_{VES}), FDA metabolites (FMET, the sum total of FDOPAC and FHVA), and 3-OMFD. 6F-3MT and FDA-sulfate were not represented as they were not detected in the brain tissue assay. For both Models I and II it is assumed that FDA is slowly released from vesicles, then following release, is rapidly metabolized via MAO and COMT to produce FDOPAC and FHVA, which may then be cleared from the

Table 2. Percentages of radiolabeled FDOPA metabolites measured in the brains of four monkeys

	Time(min)	Monkey	FDOPA	FDASULF	3-OMFD	FDOPAC	FDA	FHVA
Caudate	30	M2	5.9	0.6	19.0	14.9	39.2	20.4
	30	M3	3.8	0.1	36.6	11.3	32.8	15.4
	90	M1	0.0	1.7	42.1	2.4	11.0	42.9
	90	M4	0.0	0.4	45.1	2.4	17.4	34.7
Putamen	30	M2	6.3	0.1	29.6	9.3	41.9	12.8
	30	M3	4.6	0.1	31.8	11.8	42.6	9.1
	90	M1	1.9	0.0	32.6	5.9	26.1	33.4
	90	M4	4.2	0.0	36.1	0.0	36.0	23.6
Frontal	30	M2	17.5	4.8	69.5	8.2	0.0	0.0
	30	M3	21.0	1.4	70.0	0.0	7.6	0.0
	90	M1	5.7	2.1	73.1	2.7	9.9	6.6
	90	M4	3.9	0.0	89.1	2.1	1.2	3.7
Occipital	30	M2	17.3	4.0	73.8	2.9	1.9	0.0
	30	M3	14.3	0.0	77.0	5.2	0.8	2.7
	90	M1	5.7	5.5	68.6	3.1	6.5	10.6
	90	M4	4.5	5.3	79.9	1.6	1.6	7.0
Cerebellum	30	M2	18.4	0.7	71.5	3.6	2.5	3.3
	30	M3	14.6	0.7	79.0	1.8	1.6	2.2
	90	M1	5.4	4.8	83.6	1.1	0.0	5.1
	90	M4	7.0	0.0	90.3	0.3	0.0	2.4
Blood	30	M2	25.2	22.4	33.0	3.3	6.0	10.1
	30	M3	41.3	12.1	34.1	4.8	4.8	2.7
	90	M4	15.2	27.1	24.1	1.0	4.1	28.5

The metabolites identified were FDOPA, FDASULF, 3-OMFD, FDOPAC, FDA, FHVA. The monkeys (M1-M4) are as describe in Table 1. The second column shows the FDOPA circulation time prior to sacrifice. Blood was not assayed for monkey M1.

brain. In Model II, FDA may also be rapidly metabolized as an alternative to vesicular storage. For both models, 3-OMFD is assumed to come only from the periphery. The composite model parameters are the tissue exchange parameters for FDOPA (K_1, k_2), and 3-OMFD (K_{1M}, k_{2M}), AAAD activity (k_{AAAD}), vesicular uptake or trapping rate (k_{trap}), the slow loss rate of FDA from vesicles (k_{loss}), metabolism of free FDA (k_{met}), and the clearance of FDA metabolites from the brain (k_{CL}).

In our implementation, the compartment FDA_{FREE} and the rate constants for trapping and rapid metabolism were in fact only schematic. The rate constants were set very high, such that those compartmental components served only to divide the decarboxylation product instantaneously between the FDA_{VES} and the FMET compartments. In Model I, k_{met} was set to zero, and thus this model differed from the basic model only in that the loss of FDA_{VES} from tissue was a two step rather than a one step process. In Model II, k_{trap} and k_{met} were arbitrarily set equal, so that half the decarboxylation product entered FDA_{VES} and the other half was immediately subject to loss from the brain by the first-order process k_{cl}. In both Models I and II, the slow loss from vesicles (k_{loss}) was set to the value of k_4 estimated using the basic model of Figure 2, and the four parameters K_1, k_{AAAD}, k_{CL}, and V_b were determined by fitting the striatum TAC from 0-120 minutes. The fractions of the individual metabolites at 30 and 90 minutes for Models I and II were determined and compared with the radioactive metabolite fractions measured in the tissue assay. The metabolite fractions at 60 minutes were compared to those drawn from a previous brain assay performed on *Macaca Nemestrina* monkeys (10). Although this previous study included lesioned animals, the data from the unlesioned control animals in this previous study were chosen for comparison.

4. RESULTS

4.1. Tissue assay

The fractions of radioactive metabolites measured in each monkey are summarized in Table 2. At 30 minutes post-injection, FDA accounted for 39% of the radioactivity in striatum. The striatal levels of FDOPAC and FHVA were similar to each other (9-20%) at 30 minutes, and most of the remaining activity was 3-OMFD (19-36%). At 90 minutes, the fractions of FDA and FDOPAC were decreased, whereas the fractions of FHVA and 3-OMFD were increased. FDOPA accounted for no more than 6% of the total activity at both measurement times, and very little FDA-sulfate was found. In the cortex and cerebellum, 69-85% of the total activity was 3-OMFD. FDOPA accounted for 14-21% of the cortical activity at 30 minutes, but only 4-7% at 90 minutes. In blood plasma,

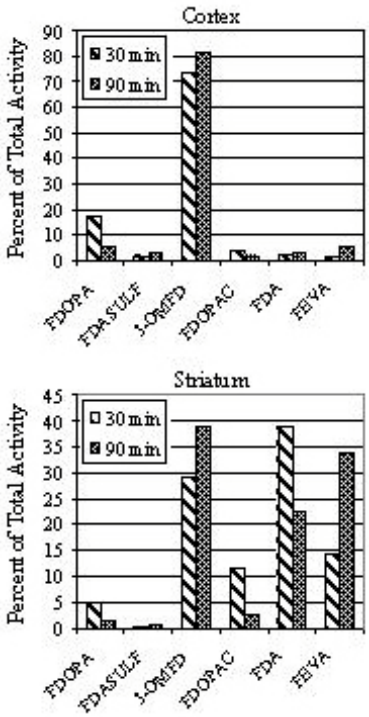

Figure 4. The fractions of FDOPA and its radioactive metabolites measured at 30 and 90 minutes post-injection. The values in striatum were obtained by averaging the radioactive metabolite fractions in caudate and putamen shown in Table 2. Those in cortex were obtained by averaging the radioactive metabolite fractions in frontal cortex, occipital cortex, and cerebellum shown in Table 2.

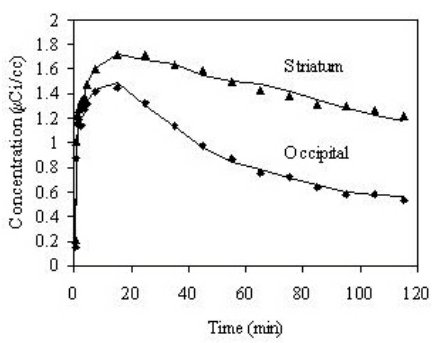

Figure 5. Data points show striatum and cerebellum time-activity curves from an FDOPA study in a rhesus monkey pretreated with 5mg/kg carbidopa. The solid lines are model fitted curves from Model II (Figure 3), but are indistinguishable from those of the basic model (Figure 2).

FDOPA and 3-OMFD each constituted about a third of the activity at 30 minutes. Most of the remaining activity was FDA-sulfate (12-22%). At 90 minutes, 3-OMFD, FDA-sulfate, and FHVA each accounted for about 25% of the plasma radioactivity, and FDOPA accounted for 15%. The high plasma concentrations of FHVA may be due to incomplete inhibition of peripheral decarboxylase, as the carbidopa dose used here (2 mg/kg) is less than the 5 mg/kg dose that is typically given to a rhesus monkey. The mean fractions of FDOPA and its metabolites in striatum (caudate, putamen), and cortex (cerebellum, frontal cortex, occipital cortex) are plotted in Figure 4. These averaged metabolite profiles were taken to be the target profiles for evaluating consistency with compartmental models of FDOPA metabolism.

4.2. Compartmental modeling

Model fitting of the TAC from occipital cortex yielded $V_e = 0.93$, and $K_1/K_{1M} = 1.5$. With these values, the predicted levels of 3-OMFD in cortex at 30 and 90 minutes were 37% and 80%, respectively. The discrepancy between the model predicted level of 3-OMFD at 30 minutes (37%), and the tissue assay (73%), will be considered in the discussion. The basic model of Figure 2 was sufficient to describe FDOPA kinetics in striatum , and gave parameter estimates of $K_1 = 0.048$ mL/min/mL, $k_3 = 0.05$ min^{-1}, $k_4 = 0.0072$ min^{-1}, and V_b=0.063 mL/mL. For Model I the fixed parameters were $V_e = 0.93$, $k_{trap} = 10^8$, $k_{loss} = 0.0072$ min^{-1}, $k_{met} = 0$, and $K_1/K_{1M} = 1.5$, and the fitted parameter values were $K_1 = 0.047$ mL/min/mL, $k_{aaad} = 0.047$ min^{-1}, $k_{cl} = 0.19$ min^{-1}, and $V_b = 0.062$ mL/mL. For Model II, parameters were fixed as for Model I, except $k_{met} = k_{trap} = 10^8$. The fitted parameters for Model II were K_1=0.047 mL/min/mL, $k_{aaad} = 0.054$ min^{-1}, $k_{cl} = 0.0153$ min^{-1}, and V_b=0.062 mL/mL. Note that for applying each model (basic model, Models I and II) to a striatum TAC, there were four fitted parameters, and all gave nearly identical residual sum of squares. Similarly, the predicted model curves were visually indistinguishable from each other. The model curve shown in Figure 5 is from Model II, but is equally representative of the other two models. Therefore, all models are equally consistent with FDOPA kinetics as measured by PET. The corresponding metabolite fractions that are predicted by Models I and II are shown in Table 3. The most obvious discrepancy is that Model I predicted a very small FMET fraction, whereas Model II predicted a much larger FMET fraction that was more consistent with the tissue assay. Compared to Model I, FDA levels predicted by Model II were also in better agreement with the tissue assay. Both models gave similar predictions of FDOPA and 3-OMFD, which were mostly consistent with the tissue assay except for the larger FDOPA fraction predicted at 30 minutes.

5. DISCUSSION

A discrepancy has previously been found in the FDOPA metabolite fractions measured in rat striatum, and those predicted by a compartmental model of FDOPA (14). In particular, the striatal fraction of FDOPAC for at least the first ten minutes following FDOPA was larger than was predicted by the model. The authors proposed that there was a delay in the vesicular storage of FDA, such that some newly synthesized FDA is metabolized via MAO before it can be trapped in vesicles. This is consistent with the notion that dopamine synthesized from exogenous L-DOPA, which bypasses the rate limiting tyrosine hydroxylase (TH) step, is handled differently from endogenous L-DOPA formed from dietary tyrosine. Dopamine storage is functionally involved in regulating TH activity by controlling the inhibition of TH by its end-product (25). This control is made possible by the close

Table 3. Comparison of the striatal FDOPA metabolite fractions predicted by Models I and II and measured in tissue

Method	Time	FDOPA	FDA	FMET	3-OMFD
Tissue assay	30 min	5.1	39.1	26.2	29.2
Model I		20.5	50.6	1.7	27.3
Model II		18.6	27.3	27.0	27.2
Melega *et al.*1991, (10)	60 min	8.0	35.0	22.0	35.0
Model I		5.5	60.0	2.2	32.8
Model II		4.9	31.7	30.7	32.7
Tissue assay	90 min	1.5	22.6	36.4	39.0
Model I		2.4	58.7	2.2	36.8
Model II		2.1	31.3	29.8	36.8

The percent fractions of FDOPA and its metabolites predicted by Model II that correspond to the fitted striatum curve in Figure 5. FMET is the sum total of FDOPAC and FHVA. The tissue metabolite fractions at 30 and 90 minutes, which were measured in the present study, are the same values that are plotted in Figure 4. The tissue data at 60 minutes shows the metabolite fractions in putamen from a study in normal Macaca Nemestrina monkeys (10).

physical proximity of TH with storage vesicles (26). Since intraneuronal AAAD is more ubiquitous, a pool of AAAD near the TH-vesicles structures can form the slow turnover FDA while more distant AAAD makes it possible for MAO to intercept FDA before protection by storage is possible, thus forming the fast turnover FDA pool. Consistent with this conjecture, in the present study we found large fractions of FDOPAC and FHVA in primate striatum within 30 minutes of FDOPA injection, indicating that some FDA is exposed to rapid turnover. Consequently, a model that assumed only slow FDA turnover (Model I) predicted much smaller levels of FDA metabolites than were measured in the tissue assay. By including a rapid component of FDA turnover, Model II was better able to match the observed levels of FDA metabolites. Thus, in agreement with the previous finding in rats, we find in primate that two distinct rates of FDA turnover are needed to bring the model predictions into reasonable consistency with both tissue kinetics and tissue metabolites.

It is important to note that the compartmental modeling exercise reported here was not intended to suggest an improvement or refinement of the models used to reduce the data from PET FDOPA studies. On the contrary, our results make it clear that the striatal time course data simply will not support any model of greater complexity than that in Figure 2. The model described in Figure 3, with the probabilities of vesicular storage and rapid metabolism arbitrarily set equal (Model II), reproduced the temporal profile of metabolite appearance remarkably well (Table 3); however, there was at the same time no measurable change in the optimal striatal fit. Interestingly, despite the very different fates of FDA in the basic model and in Model II, the rate constants corresponding to decarboxylation (k_3 and k_{aaad} respectively) differed from each other by only 5 percent. Similarly, the total equilibrium distribution volumes of all post-decarboxylation products, calculated from the model rate constants by conventional methods, differed by only 3 percent. Thus the two models were in agreement, at least over the 120 min study duration, about both the rate of uptake into a slow kinetic component and the effective rate of reversibility or loss from this component, despite the splitting of this component into two parts in Model II.

The identical nature of the striatal time courses predicted by these very different models does not detract from the utility of FDOPA imaging for the assessment of disease progression. The concept that the striatal kinetics of FDOPA can be most usefully interpreted in terms of first, the rate of incorporation into an extra tissue capacity for the tracer that is not present in non-dopaminergic regions, and second, the rate of turnover of that capacity, has been formalized in a series of reports from the University of British Columbia (27-29). The ratio of uptake rate constant to loss rate constant represents a quantitative measure of the equilibrium distribution volume of all of the products of decarboxylation. This volume was found to correlate well with classic *in vitro* indices of dopamine turnover and metabolism measured post mortem in nonhuman primates (28), and may prove to be a sensitive and specific indicator of disease progression (30). As it is the ratio of uptake to loss, this volume is simultaneously sensitive to changes in either process. It thus extends information about decarboxylation rates of FDOPA, and by inference of therapeutic L-DOPA, by providing a measure of the availability of the decarboxylation products over time following a single administration. Decarboxylase activity may be relatively spared as disease progresses (31), thus reducing its specificity to disease progression. A reduction in distribution volume that exceeds the reduction in decarboxylation rate in the same patient indicates that the dwell time of decarboxylation products in tissue has been reduced (30). Thus any data reduction method that successfully quantifies both the uptake of FDOPA into an excess tissue capacity, and the dwell time or persistence of that extra capacity over time, will draw most of the useful information from the measured data, regardless of the actual complexity of the tracer kinetics.

Our confirmation that a significant fraction of the FDOPA dose has appeared as catabolic products of FDA as early as 30 minutes post-administration strongly implies that this is also the fate of L-DOPA. It is our hypothesis

that the corresponding dopamine, appearing early but unprotected, is nonetheless 'effective'. Contin *et al.* (32) investigated the duration of the therapeutic effect of individual L-DOPA doses in patients determined clinically to be either stable or fluctuating in their response to L-DOPA treatment. Fluctuating patients had a therapeutic benefit, as determined by a finger-tapping exercise, that compared favorably to that of non-fluctuating patients in terms of magnitude, but with a greatly reduced duration. As the total tissue concentration of storage vesicles is progressively diminished, it is possible that the pharmacodynamics of therapeutic L-DOPA become dominated by the passage of the unprotected, rapidly metabolized kinetic component implied by our results.

Finally, our results bear on the important issue of COMT activity in brain. There were roughly equal amounts of FDOPA and 3-OMFD in the blood at 30 minutes, while at the same time there was over four times as much 3-OMFD than FDOPA in cortical tissue. This cannot be explained by the blood-tissue exchange kinetics of these compounds. Although 3-OMFD is extracted somewhat more rapidly than FDOPA, they have similar volumes of distribution (33,34). Thus the relative tissue levels of FDOPA and 3-OMFD indicate the central metabolism of FDOPA to 3-OMFD, either during the extraction process or in the brain tissue itself. This has been suggested by the ability of a centrally acting COMT inhibitor to effect greater reduction of 3-OMFD production than a peripheral COMT inhibitor (35). Because of these indications, it is not surprising that there was lack of agreement between the measured FDOPA and 3-OMFD levels at 30 minutes, and those predicted by compartmental models that neglect central COMT activity. It is important to note that despite the evidence for central 3-OMFD production the percentages shown in Table 2 indicate a remarkable uniformity of the total radioactivity associated with 3-OMFD (regional percentage times regional total radioactivity concentration) across brain regions, giving strong support to data analysis methods that depend on that assumption.

6. REFERENCES

1. Gjedde A., J. Reith, S. Dyve, G. Leger, M. Guttman, M. Diksic, A. Evans & H. Kuwabara. Dopa decarboxylase activity of the living human brain. *Proceedings of the National Academy of Sciences of the United States of America* 88, 2721-2725 (1991)
2. Huang S.-C., D.-C. Yu, J. R. Barrio, S. Grafton, W. P. Melega, J. M. Hoffman, N. Satyamurthy, J. C. Mazziotta & M. E. Phelps. Kinetics and modeling of L-6-[^{18}F]fluoro-DOPA in human positron emission tomographic studies. *Journal of Cerebral Blood Flow and Metabolism* 11, 898-913 (1991)
3. Hoshi H., H. Kuwabara, G. Leger, P. Cumming, M. Guttman & A. Gjedde. 6-[18F]fluoro-L-DOPA metabolism in living human brain: A comparison of six analytical methods. *Journal of Cerebral Blood Flow and Metabolism* 13, 57-69 (1993)
4. Kuwabara H., P. Cumming, J. Reith, G. Leger, M. Diksic, A. C. Evans & A. Gjedde. Human striatal L-DOPA decarboxylase activity estimate *in vivo* using 6-[fluoro-DOPA and positron emission tomography: error analysis and application to normal subjects. *Journal of Cerebral Blood Flow and Metabolism* 13, 43-56 (1993)
5. Wahl L. & C. Nahmias. Modeling of fluorine-18-6-fluoro-l-dopa in humans. *Journal of Nuclear Medicine* 37, 432-437 (1996)
6. Cumming P., B. E. Boyes, W. R. W. Martin, M. Adam, J. Grierson, T. Ruth & E. G. McGeer. The metabolism of [18F]6-fluoro-L-3,4-dihydroxyphenylalanine in the hooded rat. *Journal of Neurochemistry* 48, 601-608 (1987)
7. Melega W. P., A. Luxen, M. M. Perlmutter, C. H. K. Nissenson, M. E. Phelps & J. R. Barrio. Comparative *in vivo* metabolism of 6-[18F]fluoro-L-DOPA and [3H]L-DOPA in rats. *Biochemical Pharmacology* 39, 1853-1860 (1990)
8. Firnau G., S. Sood, R. Chirakal, C. Nahmias & E. S. Garnett. Cerebral metabolism of 6-[18F]fluoro-L-3,4-dihydroxyphenylalanine in the primate. *Journal of Neurochemistry* 48, 1077-1082 (1987)
9. Melega W. P., S. T. Grafton, S.-C. Huang, N. Satyamurthy, M. E. Phelps & J. R. Barrio. L-6-[^{18}F]Fluoro-DOPA metabolism in monkeys and humans: Biochemical parameters for the formulation of tracer kinetic models with positron emission tomography. *Journal of Cerebral Blood Flow and Metabolism* 11, 890-897 (1991)
10. Melega W. P., J. M. Hoffman, J. S. Schneider, M. S. Phelps & J. R. Barrio. 6-[18F]fluoro-L-DOPA metabolism in MPTP-treated monkeys: assessment of tracer methodologies for positron emission tomography. *Brain Research* 543, 271-276 (1991)
11. Garnett S., G. Firnau, C. Nahmias & R. Chirakal. Striatal dopamine metabolism in living monkeys examined by positron emission tomography. *Brain Research* 280, 169-171 (1983)
12. Barrio J. R., S.-C. Huang, D.-C. Yu, W. P. Melega, J. Quintana, S. R. Cherry, A. Jacobson, M. Namavari, N. Satyamurthy & M. E. Phelps. Radiofluorinated L-m-tyrosines: New in-vivo probes for central dopamine biochemistry. *Journal of Cerebral Blood Flow and Metabolism* 16, 667-678 (1996)
13. Endres C. J., S. Swaminathan, O. T. DeJesus, M. Sievert, A. E. Ruoho, D. Murali, S. G. Rommelfanger & J. E. Holden. Affinities of dopamine analogs for monoamine granular and plasma membrane transporters: implications for PET dopamine studies. *Life Sciences* 60, 2399-2406 (1997)
14. Deep P., A. Gjedde & P. Cumming. On the accuracy of an [18F]FDOPA compartmental model: evidence for vesicular storage of [18F]fluorodopamine *in vivo*. *J Neurosci Methods* 76, 157-165 (1997)
15. Justice Jr. J. B., L. C. Nicolaysen & A. C. Michael. Modeling the dopaminergic nerve terminal. *Journal of Neuroscience Methods* 22, 239-252 (1988)
16. Zetterstrom T., T. Sharp, A. K. Collin & U. Ungerstedt. *In vivo* measurement of extracellular dopamine and DOPAC in rat striatum after various dopamine-releasing drugs; implications for the origin of extracellular DOPAC. *European Journal of Pharmacology* 148, 327-334 (1988)
17. Soares-Da-Silva P. & M. C. Garrett. A kinetic study of the rate of formation of dopamine, 3,4-dihydroxyphenylacetic acid (DOPAC) and homovanillic

acid (HVA) in the brain of the rat: Implications for the origin of DOPAC. *Neuropharmacology* 29, 869-874 (1990)
18. Buu N. T. Vesicular accumulation of dopamine following L-DOPA administration. *Biochemical Pharmacology* 38, 1878-1892 (1989)
19. Dedek J., R. Baumes, N. Tien-Duc, R. Gomeni & J. Korf. Turnover of free and conjugated (sulphonoxy) dihydroxyphenylacetic acid and homovanillic acid in rat striatum. *Journal of Neurochemistry* 33, 687-695 (1979)
20. DeJesus O. T., C. J. Endres, S. E. Shelton, R. J. Nickles & J. E. Holden. Non-invasive assessment of aromatic L-amino acid decarboxylase activity in aging rhesus monkey brain *in vivo*. *Synapse* (2000)
21. Cumming P., H. Kuwabara & A. Gjedde. A kinetic analysis of 6-[18F]fluoro-L-dihydroxyphenylalanine metabolism in the rat. *Journal of Neurochemistry* 63, 1675-1682 (1994)
22. Cumming P., H. Kuwabara, A. Ase & A. Gjedde. Regulation of dopa decarboxylase activity in brain of living rat. *Journal of Neurochemistry* 65, 1381-1390 (1995)
23. Adam M. J. & S. Jivan. Synthesis and purification of L-6-[18F]fluorodopa. *Appl. Radiat. Isot.* 39, 1203-1206 (1988)
24. Nickles R. J., O. T. DeJesus, O. H. Solin & M. Haparaanta. A flow-through detector for nanocurie activities encountered in HPLC analysis of PET tracer metabolites. *IEEE Transactions on Nuclear Science* 39, 2316-2321 (1992)
25. McMillen B. A. & P. A. Shore. Role of dopamine storage function in the control of rat striatal tyrosine hydroxylase activity. *Naunyn-Schmeideberg's Arch. Pharmacol.* 313, 39-44 (1980)
26. Pickel V. M., T. Joh & D. J. Reis. Regional and ultrastructural localization of tyrosine hydroxylase by immunocytochemistry in dopaminergic neurons of the mesolimbic and nigroneostriatal systems. In: *Nonstriatal dopaminergic neurons.* Eds. Costa E., Gessa L.. Raven Press, New York (1977)
27. Holden J.E., D. Doudet, C.J. Endres, G.L-Y. Chan, K.S. Morrison, F.J.G. Vingerhoets, B.J. Snow, B.D. Pate, V. Sossi, K.R. Buckley, & T.J. Ruth. Graphical analysis of 6-fluoro-L-DOPA trapping: Effect of inhibition of catechol-O-methyltransferase. *Journal of Nuclear Medicine* 38: 1568-1574 (1997)
28. Doudet D.J., G.L-Y. Chan, J.E. Holden, E. McGeer, T.A. Aigner, R.J. Wyatt, & T.J. Ruth. 6-Fluoro-L-dopa PET studies of the turnover of dopamine in MPTP-induced parkinsonism in monkeys. *Synapse* 29: 225-232 (1998)
29. Sossi V. , D.J. Doudet, & J.E. Holden. A reversible tracer analysis approach to the study of effective dopamine turnover. *Journal of Cerebral Blood Flow and Metabolism* 21: 469-476 (2001)
30. Sossi V., R. de la Fuente-Fernández, J.E. Holden, D. J Doudet, J. McKenzie, A.J. Stoessl, T.J . Ruth. Increase in dopamine turnover occurs early in Parkinson's disease: evidence from a new modeling approach to PET 18 F-fluorodopa data. *Journal of Cerebral Blood Flow and Metabolism* 22: 232-239 (2002)
31. Lee C. S., A. Samii, V. Sossi, T. J. Ruth, M. Schulzer, J. E. Holden, J. Wudel, P. K. Pal, R. de la Fuente-Fernandez, D. B. Calne & A. J. Stoessl. *In vivo* positron emission tomographic evidence for compensatory changes in presynaptic dopaminergic nerve terminals in Parkinson's disease. *Annals of Neurology* 47, 493-503 (2000)
32. Contin, M., R. Riva, P. Martinelli, P. Cortelli, F. Albani, & A. Baruzzi. Pharmacodynamic modeling of oral levodopa: Clinical application in Parkinson's disease. *Neurology* 43, 367-371 (1993)
33. Doudet D. J., C. A. McLellan, R. Carson, H. R. Adams, H. Miyake, T. G. Aigner, R. T. Finn & R. M. Cohen. Distribution and kinetics of 3-O-methyl-6-[18F]fluoro-L-DOPA in the rhesus monkey brain. *Journal of Cerebral Blood Flow and Metabolism* 11, 726-734 (1991)
34. Wahl L., R. Chirakal, G. Firnau, E. S. Garnett & C. Nahmias. The distribution and kinetics of [18F]6-fluoro-3-O-methyl-L-DOPA in the human brain. *Journal of Cerebral Blood Flow and Metabolism* 14, 664-670 (1994)
35. Doudet D., G. Chan, J. Holden, B. Pate, K. Morrison, D. Calne & T. Ruth. Effects of monoamine oxidase and catechol-O-methyltransferase inhibition on dopamine turnover: a PET study with 6-[18F]L-DOPA. *Euopean Journal of Pharmacology* 334, 31-38 (1997)

Key Words: Parkinson's disease; dopaminergic pathway; 6-fluorodopa; L-DOPA; nonhuman primate

Send correspodence to: Dr Jim Holden, Departments of Medical Physics, University of Wisconsin Medical School Madison, WI 53706, Tel: 608-262-5998, Fax: 608-262-2413, E-mail: jeholden@facstaff.wisc.edu